

THE EFFECTS OF ROTATION AND STELLAR MAGNETIC FIELD IN THE NEBULAR SHAPES: LBV NEBULAE AND PNE

G. García-Segura¹, N. Langer², M. Różyczka³, M.-M. Mac Low⁴, and J. Franco¹

RESUMEN

Se reconsidera la formación de nebulosas bipolares, vía rotación estelar, y su aplicabilidad a la formación de nebulosas planetarias bipolares y nebulosas alrededor de LBV. También se reconsideran los efectos del campo magnético estelar y su aplicabilidad a la formación de nebulosas planetarias elípticas y nebulosas altamente colimadas. Se muestra, mediante simulaciones bidimensionales hidrodinámicas y magnetohidrodinámicas, que estos procesos son eficientes en la producción de bipolaridad y alta colimación.

También se discuten simulaciones magnetohidrodinámicas tridimensionales recientes, las cuales confirman que, los flujos colimados de las nebulosas planetarias se pueden obtener por colimación magnética de los vientos centrales. Estos flujos colimados se forman en la regiones polares a causa de la tensión magnética. Se propone que la formación de asas solapadas y asas desacopladas implican la existencia de dos y tres vientos, respectivamente. Por último, se muestra que los flujos colimados en rotación y las nebulosas con simetría puntual pueden ser el resultado de una estrella en precesión, gravitacionalmente acoplada con una compañera.

ABSTRACT

We review the formation of bipolar nebulae, via stellar rotation, and its application to the formation of bipolar LBV nebulae and planetary nebulae. Also, the effects of the stellar magnetic field are reviewed and applied to the formation of elliptical and highly collimated planetary nebulae. Two-dimensional hydrodynamical and magneto-hydrodynamical simulations indicate that these processes are efficient in driving bipolar and collimated outflows.

We also discuss recent 3-dimensional, magneto-hydrodynamical simulations, confirming that planetary nebula jets and ansae can be obtained by magnetic collimation of their central winds. Jets and ansae form at the polar regions due to the magnetic tension produced by the magnetized winds. It is proposed that the formation of “attached” and “detached” ansae involves two and three winds, respectively. It is shown that rotating jets and point-symmetric nebular shapes can be the result of a precessing star, tidally coupled with a companion.

Key words: HYDRODYNAMICS — ISM: JETS AND OUTFLOWS — PLANETARY NEBULAE: GENERAL — STARS: AGB, POST-AGB — STARS: MASS LOSS — STARS: VARIABLES: OTHER (LUMINOUS BLUE VARIABLES)

1. INTRODUCTION

It is commonly accepted that the formation of circumstellar nebulae involves the action of at least two interacting stellar winds, for both planetary nebulae (PNe) (Kwok, Purton, & Fitzgerald 1978; Kwok 1982, 1994; Kahn 1983; Balick 1987; Aller 1993) and ring nebulae around Pop I massive stars (García-Segura & Mac Low 1995).

¹Instituto de Astronomía, UNAM, Apdo Postal 70-264, 04510 México D. F., México; ggs@bufadora.astrosen.unam.mx; pepe@astroscu.unam.mx.

²Institut für Theoretische Physik und Astrophysik, Universität Potsdam, D-14415 Postdam, Germany; ntl@leo.astro.physik.uni-potsdam.de.

³Warsaw University Observatory, Al. Ujazdowskie 4, 00-478 Warszawa, Poland; also N. Copernicus Astronomical Center, Bartycka 18, 00-716 Warszawa, Poland.

⁴Max-Planck-Institut für Astronomie, Königstuhl 17, D-69117 Heidelberg, Germany.

Chu (1993) extensively showed that PNe and ring nebulae around massive stars are not only similar in morphologies. For massive stars that evolve through red supergiant (RSG), or luminous blue variable (LBV) phases towards a Wolf-Rayet (WR) phase, the final WR fast wind would sweep up the slow RSG or LBV wind and form a bubble of stellar material, reminiscing the two-wind formation of PNe. Sometimes, as Chu pointed out, it can be really difficult to determine whether the central star of a ring nebula is a PN nucleus or a Pop I massive star. In fact, many ring nebulae around massive stars were once cataloged as PNe, e.g., AG Car (PK 289-0°1) and NGC 6164-5 (PK 336-0°1), and also, there are nebulae classified alternately as PNe and ring nebulae, e.g., M1-67 and We21.

It has been shown by Langer (1997) and by García-Segura et al. (1998) that both LBVs and asymptotic giant branch (AGB) stars reach the Ω -limit of critical rotation, independently of the actual stellar rotation rate. García-Segura et al. (1997, 1998) and Langer, García-Segura, & Mac Low (1997) have shown that the result is a slow, massive, equatorially confined outflow, which may be inflated to a double lobe structure by a fast spherically symmetric wind later on. The striking similarity of the shapes of some PNe and LBV nebulae —e.g., compare the “Hourglass Nebula” MyCn18 with the “Homunculus Nebula” surrounding η Carinae— is certainly in support of the view that they have a common underlying physical principle. This is in line with an earlier suggestion by Calvet & Peimbert (1983) that the bipolar nature of Type I nebulae (Peimbert 1978) could be explained in terms of rather massive, fast rotating progenitors ($M_i \geq 2.4 M_\odot$) that had to lose an appreciable fraction of their mass and angular momentum during the PN phase. In such a case, the main cause of bipolarity would be stellar rotation.

Asymmetries of the precursor AGB wind are not the only factor responsible for the shaping of PNe. Based on a thin shell approximation, Chevalier & Luo (1994) obtained self-similar models of aspherical nebulae produced by a rotating star with a *magnetized* fast wind. Their procedure did not include asymmetries of the AGB wind, and the aspherical shapes were due solely to the tension of the toroidal magnetic field. Recent MHD simulations by Różyczka & Franco (1996) (2-dimensional, cylindrical calculations) and by García-Segura et al. (1998) (2-dimensional, spherical calculations) have shown that magnetic effects may also be responsible for the generation of collimated flows (jets) observed in some nebulae.

One should note that two-dimensional calculations in either cylindrical or spherical coordinate systems could induce spurious effects at the rotation axis, because the axis in these coordinate systems is a geometrical singularity, i.e., the gas is not allowed to pass through it. The only possible way to clarify the possible existence of an “axis problem” is by using 3-dimensional cartesian grids. This choice allows to locate the star in the middle of the computational volume. The 3-D computations performed by García-Segura (1997) show that the behavior of the gas is similar to those computed in 2-dimensions, with the only difference that the collimated gas can be subject to kink instabilities. Thus, the formation of jets and ansae are confirmed in 3-dimensional, axis-free, calculations.

2. THE EFFECTS OF STELLAR ROTATION: THE OMEGA LIMIT

In the Hertzsprung-Russell diagram, LBV stars like η Car lie close to the upper borderline of temperature and luminosity beyond which no normal stars are observed (Humphreys & Davidson 1979), near the location of the Eddington limit.

As Figure 1 shows, a massive star expanding at constant luminosity due to an opacity increase in its surface layers. The Eddington limit is reached when $\Gamma = L/L_{\text{Edd}} = 1$, where the Eddington luminosity $L_{\text{Edd}} = 4\pi cGM/\kappa$, with c the speed of light, M and L the mass and luminosity of the star, and κ the opacity at the stellar surface. Note that when $\Gamma \rightarrow 1$, the escape velocity $v_{\text{esc}} = [(1 - \Gamma)2GM/R]^{1/2} \rightarrow 0$. This implies a very slow wind velocity ($\simeq 0$) at the Eddington limit. Thus, when a star passes through a close approach to the Eddington limit, its stellar wind will follow a *fast—slow—fast* sequence.

The critical rotational velocity, where the combination of radiation pressure and centrifugal force exceeds surface gravity at the equator, given by $v_{\text{crit}} = [(1 - \Gamma)GM/R]^{1/2}$, has the same behavior as v_{esc} , i.e., when $\Gamma \rightarrow 1$, $v_{\text{crit}} \rightarrow 0$. However, the rotational velocity v_{rot} is always finite. That is, critical rotation occurs *before* the Eddington limit is reached. This is the so called *Omega limit* (Langer 1997). Winds with mass loss rates large enough to halt and reverse the stellar expansion are thought to occur when $\Omega = v_{\text{rot}}/v_{\text{crit}}$ approaches unity (Friend & Abbott 1986; Bjorkman & Cassinelli 1993). Thus, outflows will always occur before the star reaches its Eddington limit, acting to prevent further expansion.

Using this idea, we simulate the LBV outburst phenomenon by allowing the star to pass through three successive stages —pre-outburst, outburst and post-outburst— with correspondingly different stellar winds. The simulations were performed with the hydrodynamic code ZEUS, developed by M. L. Norman and the Laboratory

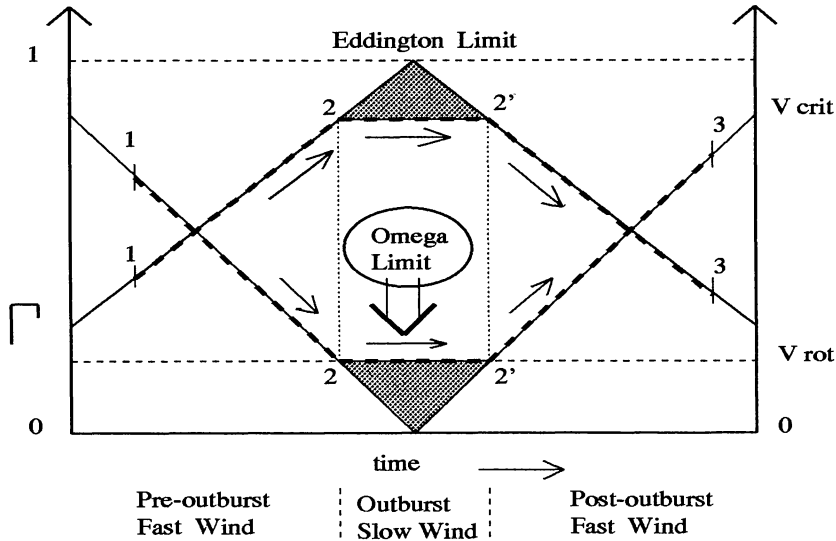


Fig. 1. Time evolution of the Eddington factor Γ and the critical rotation velocity v_{crit} . For simplicity, we assumed a constant equatorial rotational velocity v_{rot} (dashed line). As discussed in the text, the outburst (2–2') will occur before the star reaches its Eddington limit (dashed line), at the Omega limit.

for Computational Astrophysics (Stone & Norman 1992). See García-Segura, Mac Low, & Langer (1996) for further details about our numerical method. To include the effects of stellar rotation on the winds, we use the analytic model of Bjorkman & Cassinelli (1993), with stellar parameters appropriate to η Car [$M = 80 M_{\odot}$, $\log(L/L_{\odot}) = 6.4$, and $\log T_{\text{eff}} = 4.2$ ($\Rightarrow R = 210 R_{\odot}$) at the outburst]. We use a wind velocity law with $\beta = 3$, which appears appropriate for the case of a very dense wind (Cassinelli, Ignace & Bjorkman 1995), and appropriate values for the other parameters of the problem (Bjorkman & Cassinelli 1993): $\zeta = 1$, $\gamma = 0.35$, and $\xi = -0.43$.

We compute the hydrodynamic evolution of the circumstellar gas, starting our computations at the beginning of the giant outburst in 1840 A.D., and run them until 1996 A.D.. We show in Figure 2 (Plate 1) two models at 1996 A.D. with different assumptions about the stellar wind parameters, as described below. However, our main results depend only on our basic outburst scenario: the star is close to its Eddington limit during outburst (1840–1860 A.D.; 2–2' in Fig. 1), but is hotter, more compact, and thus further away from the Eddington limit before and after outburst (1,3 in Fig. 1). The smaller value of Γ before and after the outburst has two consequences: larger wind velocities due to larger escape velocities *and* smaller values of Ω leading to more spherical winds.

Model A. Pre-outburst: $\dot{M} = 10^{-3} M_{\odot} \text{ yr}^{-1}$, $v_{\infty, \text{pole}} = 450 \text{ km s}^{-1}$, $\Omega = 0.53$, $\Gamma \ll 0.5$. Outburst: $\dot{M} = 7 \times 10^{-3} M_{\odot} \text{ yr}^{-1}$, $v_{\infty, \text{pole}} = 269 \text{ km s}^{-1}$, $\Omega = 0.98$, $\Gamma = 0.5$. Post-outburst: $\dot{M} = 1.7 \times 10^{-4} M_{\odot} \text{ yr}^{-1}$, $v_{\infty, \text{pole}} = 1800 \text{ km s}^{-1}$, $\Omega = 0.13$, $\Gamma \ll 0.5$. The Homunculus mass is $\sim 0.15 M_{\odot}$ (according to van Genderen & Thé 1984). **Model B.** Pre-outburst: same as model A. Outburst: $\dot{M} = 5 \times 10^{-2} M_{\odot} \text{ yr}^{-1}$ (rest as model A). Post-outburst: $\dot{M} = 3 \times 10^{-3} M_{\odot} \text{ yr}^{-1}$, $v_{\infty, \text{pole}} = 800 \text{ km s}^{-1}$, $\Omega = 0.3$. The Homunculus mass is $\sim 1 M_{\odot}$.

Our outburst scenario leads to a characteristic distribution of the circumstellar gas. The initial fast wind (1 in Fig. 1) forms the background for the subsequent development of the nebula. During outburst (1840–1860 A.D.; 2–2'), the wind becomes slow and dense, and the stellar rotation concentrates it toward the equatorial plane (Bjorkman & Cassinelli 1993; Cassinelli et al. 1995). A rarefaction wave produced by the previous pre-outburst wind makes the slow wind to expand up to much larger dimensions (this wave is visible at the border of the wind-compressed equatorial zone in Fig. 2 (Plate 1)). When the final fast wind (3 in Fig. 1) starts, it sweeps up the dense wind from the outburst into a thin, radiatively cooled shell that fragments due to dynamical instabilities (García-Segura et al. 1996). The shell expands more easily into the lower density wind at the poles, producing a double-lobed structure, as shown in Fig. 2 (Plate 1).

The models are not intended to exactly fit all properties of the Homunculus nebula, as we have not searched the parameter space for the best fit. We therefore, find it striking how well these models, without much fine

tuning, not only reproduce the large-scale, bipolar morphology, but also the small scale turbulent structure seen in high-resolution observations of the Homunculus (Hester et al. 1991; Ebbets 1997). We found that the large scale shapes of the resulting nebulae, shown in Fig. 2 (Plate 1), are quite similar, but the higher wind densities in model B (Fig. 2, Plate 1), right) caused the wind termination shock to be strongly radiative, with the effect of changing the Vishniac instabilities (Vishniac 1983) seen in Plate 1 (left), characterized by long wavelengths, into ram-ram-pressure instabilities (Vishniac 1994; García-Segura et al. 1996), which have a much spikier morphology and shorter wavelengths. The observations of the Homunculus (Ebbets 1997) showed basically rounded structures in the shell consistent with Model A. However, they also showed spiky comet-like structures in several parts consistent with Model B. The radio blobs (White 1997) observed in the wind could be an explanation. The inter-blob wind density could fit better with model A, but the collision of the blobs with the shell strongly enhances locally the radiative cooling, producing features as the one in model B.

What about PNe? In order to evaluate whether AGB rotation rates can produce similar situations as the one discussed above, we have to compare them with the rate of critical rotation. Besides the fact that an AGB star does not have a well defined surface, also the force balance is not yet well understood (e.g., Krüger, Gauger, & Sedlmayr 1994). This is particularly so for the phase where the PN material is actually ejected from the star, since the responsible physical processes are not yet unambiguously identified. Recent work, which refers to ideas by Lucy (1967) and Paczyński & Ziółkowski (1968), proposes a runaway expansion of the envelope, triggered by the luminosity and radius increase during a thermal pulse, and maintained by the liberation of energy by hydrogen recombination (cf., Wagenhuber & Weiss 1994; Han, Podsiadlowski, & Eggleton 1994). However, independent of the physical details, if the PN ejection is produced by the envelope approaching an instability, this means that the escape velocity and thus the critical rotational velocity approach zero. In this case, the situation is intriguingly similar to that of giant outbursts of LBVs.

This is the main reason why we think that values of Ω very close to 1 may be appropriate for AGB stars during the phase of PN ejection. As mentioned above, the force which drives the “superwind” is not yet identified, but as radiation pressure on dust grains plays a major role in driving the normal AGB winds it is a candidate for the superwind as well. Therefore, and due to the above mentioned similarity between some PNe and LBV nebulae, we parametrize the instability in the present study in the same way as we did before for the case of giant LBV outbursts, i.e., we assume that the Eddington parameter Γ is close to 1. Clearly, the source of the opacity is different in both cases, i.e., mainly scattering on free electrons in the LBV case and dust absorption in the AGB case, but radiation pressure may be important in both cases. Our approach has the advantage that the analytic formalism describing the winds of rotating stars developed by Bjorkman & Cassinelli (1993) can be applied. Note that the critique of that model by Owocki, Cranmer, & Gayley (1996) that non-radial line forces and gravity darkening need to be included in order to describe the main effects in rotating stars winds—which may be well justified for e.g., main sequence B stars—does not apply to the case of AGB stars, since line driving is irrelevant in this case and gravity darkening does not apply in convective envelopes. In fact, if radiation pressure proves to be the relevant driving force of the superwind, it may turn out to be the best application of the Bjorkman-Cassinelli model (cf., Ignace, Cassinelli, & Bjorkman 1996), which has originally been developed in the context of hot star winds.

Ignace et al. (1996) have investigated the winds of AGB stars and find considerable density contrasts to be possible even for objects which rotate with only 10% of their critical rotation rate, simply due to angular momentum conservation. Additionally, Dorfi & Höfner (1996) have found that the strong temperature dependence of the dust condensation leads to a strong amplification of initial asymmetries in the AGB wind. Therefore, a combination of both effects may allow high density contrasts even for winds of slowly rotating AGB stars.

3. THE EFFECTS OF STELLAR MAGNETIC FIELDS: THE MAGNETIC TENSION

The magnetic field in an outflowing wind can be described by two components. The toroidal component, B_ϕ , is set using the equations for a rotating star

$$B_\phi = B_s \frac{v_{\text{rot}}}{v_\infty(\theta)} \left(\frac{r_s}{r} \right)^2 \left(\frac{r}{r_s} - 1 \right) \sin\theta, \quad (1)$$

where B_s and r_s are the magnetic field strength at the stellar surface and the stellar radius, respectively.

The latter equation is a generalization of the standard formula for B_ϕ in the equatorial ($\theta = 90^\circ$) plane (see e.g., Parks 1991). $B_\phi(\theta)$ decreases with decreasing θ due to an increase in v_∞ , and the sinusoidal function

is included to cancel entirely the toroidal field component at the $\theta = 0$ axis. This generalization is obviously arbitrary but, as Różyczka & Franco (1996) have shown, the precise form of the off-equator distribution of the field is unimportant provided that the field is sufficiently strong to cause an appreciable deformation of the shocked wind region. The radial field component can be neglected (see Chevalier & Luo 1994), so the used field configuration obeys $\nabla \cdot B = 0$.

In the following, our models are identified by the dimensionless parameter σ , which is the ratio of the magnetic field energy density to the kinetic energy density in the fast wind (Chevalier & Luo 1994)

$$\sigma = \frac{B^2}{4\pi\rho v_\infty^2} = \frac{B_s^2 r_s^2}{\dot{M} v_\infty} \left(\frac{v_{\text{rot}}}{v_\infty} \right)^2. \quad (2)$$

With this approach, an example of a MHD numerical calculation, **Model C**, is shown in Fig. 2, Plate 1 (see García-Segura et al. 1998 for details). The stellar radius (R_s) is set equal to the Solar radius, and the surface magnetic field (B_s) is assumed to be 254 Gauss, resulting in $\sigma = 0.01$. This is only slightly larger than the Solar value, $\sigma_\odot = 0.009$ (Chevalier & Luo 1994). There is no information about stellar magnetic fields in the most interesting region between the AGB phase and white dwarfs. Just white dwarfs are known to have fields of up to $10^7 - 10^8$ Gauss (Schmidt 1989). So, stellar field intensities between the solar value ($B_s = 2$ Gauss) and 10^8 Gauss are acceptable for modelling. The other wind parameters involved in the calculations are: $\dot{M}_{\text{AGB}} = 1 \times 10^{-6} M_\odot \text{ yr}^{-1}$, $\dot{M}_{\text{fast}} = 4 \times 10^{-7} M_\odot \text{ yr}^{-1}$, $v_{\infty, \text{AGB}} = 10 \text{ km s}^{-1}$, $v_{\infty, \text{fast}} = 500 \text{ km s}^{-1}$.

Model C is an example of a nonrotating AGB wind ($\Omega = 0$) which, in the absence of a magnetic field, will evolve into an spherical nebula once that the fast wind is turned on. The general effect of the magnetic field is the elongation of the nebula in the polar direction. The mechanism responsible for the elongation was described by Różyczka & Franco (1996), and only the basic points are listed here. First, the outer part of the magnetized shocked wind region becomes magnetically rather than thermally supported, i.e., the magnetic energy density gets larger than the thermal energy density (the latter decreases due to the expansion of the nebula and due to the fact that work must be done against the tension of the toroidal field). Second, the tension of the toroidal field slows down the expansion in the direction perpendicular to the symmetry axis, while the expansion in the direction parallel to the axis proceeds unimpeded. Third, a flow from the equatorial parts of the shocked wind region toward the symmetry axis is initiated, leading to the formation of stagnation regions at the axis and to the formation of jets. The gas arriving at the polar regions of the nebula forms relatively dense blobs which can be identified with the ansae observed in PNe such as NGC 6905.

When the AGB wind is modify by stellar rotation, all the effects described above have an impact in the evolution of the nebula. Moreover, when the magnetic effect is stronger than in the previous model (i.e., when σ gets larger values) a much higher degree of collimation is achieved. As an example, in **Model D** (Fig. 2, Plate 1) the surface magnetic field amounts to 802 Gauss, resulting in $\sigma = 0.1$. The other wind parameters are similar to those of model C, but now $\Omega = 0.98$ for the AGB wind. In this simulation, a bipolar nebula is also produced. However, the magnetized shocked wind is so strongly collimated that it blows out of the nebula as a pair of jets. Our models match pretty well the morphologies of M2-9 (Schwarz et al. 1996) and He 2-437 (Manchado et al. 1996).

4. 3-D MHD MODELS: JETS, ANSAE AND POINT-SYMMETRY

The 3-D simulations have been also performed with the magneto-hydrodynamic code ZEUS-3D. The computations are done in cartesian coordinates (x, y, z), with outflowing outer boundary conditions. The models have grids of $100 \times 100 \times 200$ zones in x, y and z respectively, with an extent of $0.1 \times 0.1 \times 0.2$ pc. In all models, the star is located at the center of the computational volume. The winds are set again using the equations given by Bjorkman & Cassinelli (1993).

The first 3-D computation, **Model E** (Figure 3, Plate 2), is done with two steady winds, in which the AGB wind has a $\dot{M} = 10^{-6} M_\odot \text{ yr}^{-1}$ and a $v_\infty = 10 \text{ km s}^{-1}$, with $\Omega = 0.89$, and the magnetized fast wind has a $\dot{M} = 10^{-7} M_\odot \text{ yr}^{-1}$ and a $v_\infty = 100 \text{ km s}^{-1}$, with $\sigma = 0.02$. The plates shows the integral of the emission measure projected onto the plane of the sky. This model shows how efficient is the tension of the toroidal magnetic field in making a jet. Note that the jet already forms inside of the bubble, and it is subject to kink instabilities. The reason why this model forms jets instead of attached ansae is due to the strong radiative cooling that a 100 km s^{-1} shock produces. Model C already showed the formation of attached ansae, such as the one observed in K 3-3 (Manchado et al. 1996).

Note that a nebula such as NCG 7009 or NGC 6826 shows that the ansae are detached from the main shell. In order to produce “detached” ansae, it is necessary to introduce a third wind between the AGB wind and the fast wind. This third wind, which is faster than the AGB wind, is magnetized, and behaves similarly to the one describe above. In this case, the ansae form in the transition between the AGB wind and the fast wind, where the fast wind is responsible for making the main swept-up shell.

An example of a 3-wind computation is shown in **Model F** (Fig. 3, Plate 2). The wind velocities follows the sequence 10 — 15 — 100 km s⁻¹, whereas the mass loss rates are 10⁻⁵—10⁻⁶—10⁻⁶ M_⊙ yr⁻¹. In the second wind, $\sigma = 0.03$. This requires only 36 Gauss at the stellar surface for a rotation of 1 km s⁻¹. The figure is a two-color composite synthetic picture, where red represents the low excitation material ([N II]), and green is the high excitation, photoionized gas (H_α, [O III]). Note that the calculation includes an approximation for the photoionization, where $\log F_{\star} = 46.5s^{-1}$ is the rate of ionizing photons. In this model, the ansae are clearly detached from the main nebula. Note that the reason why the ansae appears in red ([N II]) is due to the trapping of the ionization front in the densest blobs.

4.1. Precessing Cases: Point-Symmetry

The previous sections describe how the material is collimated toward the polar regions by the hoop stress. Since, the toroidal magnetic field carried out by the wind follows the rotation axis of the central star, it is now tempting to include a precession in the rotation axis. The simplest idea is to include the precession caused by a companion, *which does not mean a close companion*. It is easy to imagine the topology of the magnetic field lines in such a scenario, i.e., multiple magnetic rings centered along the spin axis of the star (Figure 4). As the axis changes its orientation, the rings also change their orientation. This idea is very attractive, since it is known that 50 % of the solar type stars are binaries, but not close companions.

In order to illustrate how the precession can produce interesting effects, we have computed a model similar to model E, i.e., with the same wind parameters but including a precession with a period of 4000 yr, and a precession angle of 18°. The result is shown in **Model G** (Fig. 3, Plate 2). Note that a pair of rotating jets are formed in this simulation. However, the pattern of the jets does not follow exactly the motion caused by the precession. In fact, the behavior is more chaotic because of the kink instabilities, making it difficult to recover the precession period from the figure.

There are also cases in nature where not only the ansae appear detached from the main nebula, but also they present point-symmetry. For example, the nebulae J320 and IC 4634 are typical examples of point-symmetric shapes. It is hard to imagine a mechanism that can produce such a shape. In fact, many authors have made efforts to reproduce such a shape without success. The scenario described here, the magnetic collimation with precession can produce “naturally” those shapes.

Model H (Fig. 3, Plate 2) is a computation which includes 3-winds, as model F, but using the same technique as model G. Here, the winds follow the velocities 10 — 80 — 200 km s⁻¹, with 10⁻⁶ — 10⁻⁶ — 10⁻⁷ M_⊙ yr⁻¹ respectively. In the second wind, $\sigma = 0.02$. The period of the precession is 2000 yr, with a precession angle of 10°. The figure is again displayed in a two-color synthetic mode. The most interesting result from this simulation is that the major axis of the main nebula is completely misaligned from the line connecting the ansae, almost 45°, such as in the case of J320 and IC 4634.

5. SUMMARY

Our model moves well beyond other recent hydrodynamic models for LBV nebulae by directly tying the outburst—the visual maximum in the LBV light curves—to the equatorially confined slow wind. Earlier models (Nota et al. 1995; Frank, Balick, & Davidson 1995) concluded that a strong equatorial density enhancement must have existed before the outburst occurred. In contrast, we obtain self-consistently from our model not only the two lobes, with their small-scale structure, but also the equatorial density enhancement, and relate both to the evolutionary state of the star.

We find that our proposed scenario for giant LBV outbursts in rotating, massive, single stars leads naturally to a circumstellar gas distribution strikingly similar to the Homunculus nebula of η Car. This is so because stars with a finite rotation velocity arrive at critical rotation when they approach their Eddington limit. The clear bipolar nature of virtually all LBV nebulae (Nota et al. 1995), as well as the progressive, more-spherical morphology that LBV nebulae observations reveal inside of an evolutionary dynamical sequence (Nota & Clampin 1997), lend strong support to this scenario.

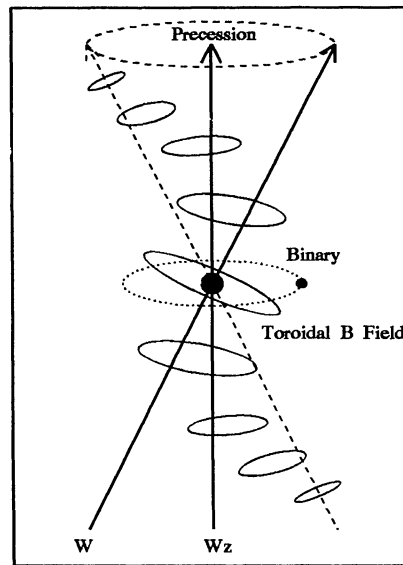


Fig. 4. Magnetic field configuration emerging from the precessing star.

We found also that the same mechanism can be applied for the most massive PN progenitors, giving rise to the formation of classical bipolar planetary nebulae.

Magnetized fast winds produce elongated PNe even from symmetrical AGB winds. By combining the effects of rotation and magnetic fields, it is possible to obtain highly collimated bipolar nebulae. In particular, strong fields and aspherical winds from rotating AGB stars can account for the origin of jets and “flyers”.

We propose that the formation of “attached” and “detached” ansae involves two and three winds respectively.

The origin of rotating jets and point-symmetric nebular shapes can be explained by the result of a precessing star, tidally coupled with a companion, inside of the framework of the magnetic collimation.

Plates 1 and 2 are available at the anonymous ftp server kepler.astroscu.unam.mx, cd papers/ggs.

We thank C. Allen, A. Arrieta, J. Fliegner, G. Koenigsberger, A. López, A. Manchado, S. Owocki, M. Peimbert, S. Torres-Peimbert, and S. White for useful comments and discussions. We also thank M. L. Norman and the Laboratory for Computational Astrophysics for the use of ZEUS-3D. The computations were performed at Instituto de Astronomía-UNAM, Instituto de Astrofísica de Canarias, the Supercomputer Center of the Universidad Nacional Autónoma de México, Rechenzentrum Garching of the Max-Planck-Gesellschaft and Instituto Nacional de Astrofísica, Óptica y Electrónica. This work was partially supported by DGAPA-UNAM grant IN105894, CONACyT grant 400354-5-4843E, and by a R&D CRAY Research grant. M.R. acknowledges the support from the Committee for Scientific Research through the grant 2P 304 017 07.

REFERENCES

- Aller, L. H. 1993, in IAU Symp. 155, Planetary Nebulae, ed. R. Weinberger & A. Acker (Dordrecht: Kluwer), 1
 Balick, B. 1987, *AJ*, 94, 671
 Bjorkman, J. E., & Cassinelli, J. P. 1993, *ApJ*, 409, 429
 Calvet, N., & Peimbert, M. 1983, *RevMexAA*, 5, 319
 Cassinelli, J. P., Ignace, R., & Bjorkman, J. E. 1995, in IAU Symp. 163, Wolf-Rayet Stars: Binaries, Colliding Winds, Evolution, ed. K. A. van der Hucht & P. M. Williams, (Dordrecht: Kluwer), 191
 Chevalier, R. A., & Luo, D. 1994, *ApJ*, 421, 225
 Chu, Y.-H. 1993, in IAU Symp. 155, Planetary Nebulae, ed. R. Weinberger & A. Acker, (Dordrecht: Kluwer), 139
 Dorfi, E.A., & Höfner, S. 1996, *A&A*, 313, 605

- Ebbets, D., Morse, J., Davidson, K., & Walborn, N. 1997, in ASP Conf. Ser. 120, Luminous Blue Variables: Massive Stars in Transition, ed. A. Nota & H.J.G.L.M. Lamers, (San Francisco: ASP), 249
- Frank, A., Balick, B., & Davidson, K. 1995, ApJ, 441, L77
- Friend, D. B., & Abbott, D. C. 1986, ApJ, 311, 701
- García-Segura, G. 1997, ApJ, 489, L189
- García-Segura, G., & Mac Low, M.-M. 1995, ApJ, 455, 160
- García-Segura, G., Langer, N. & Mac Low, M.-M. 1997, in ASP Conf. Ser. 120, Luminous Blue Variables: Massive Stars in Transition, ed. A. Nota & H.J.G.L.M. Lamers, (San Francisco: ASP), 332
- García-Segura, Mac Low, M.-M., & Langer, N. 1996, A&A 305, 229
- García-Segura, G., Langer, N., Różyczka, M., & Franco, J. 1998, in preparation.
- Han, Z., Podsiadlowski, P., & Eggleton, P. P. 1994, MNRAS 270, 121
- Hester, J. J., Light, R. M., Westphal, J. A., Currie, D. G., Groth, E. J., Holtzmann, J. A., Lauer, T. R., & O'Neil, E. J. Jr. 1991, AJ, 102, 654
- Humphreys, R. M., & Davidson, K. 1979, ApJ, 232, 409
- Ignace, R., Cassinelli, J. P., & Bjorkman, J. E. 1996, ApJ, 459, 671
- Kahn, F. D. 1983, in IAU Symp. 103, Planetary Nebulae, ed. D. R. Flower (Dordrecht: Kluwer), 305
- Krüger D., Gauger A., & Sedlmayr E. 1994, A&A 290, 573
- Kwok, S. 1982, ApJ, 258, 280
- _____. 1994, PASP, 106, 344
- Kwok, S., Purton, C. R., & Fitzgerald, P. M. 1978, ApJ, 219, L125
- Langer, N., García-Segura, G., & Mac Low, M.-M. 1998, ApJ (Letters), submitted
- Langer, N. 1997, in ASP Conf. Ser. 120, Luminous Blue Variables: Massive Stars in Transition, ed. A. Nota & H.J.G.L.M. Lamers, (San Francisco: ASP), 83
- Lucy, L. B. 1967, AJ 72, 813
- Manchado, A., Guerrero, M., Stanghellini, L., & Serra-Ricart, M. 1996, The IAC Morphological Catalog of Northern Galactic Planetary Nebulae, ed. Instituto de Astrofísica de Canarias
- Nota, A., & Clampin, M. 1997, in ASP Conf. Ser. 120, Luminous Blue Variables: Massive Stars in Transition, ed. A. Nota & H.J.G.L.M. Lamers, (San Francisco: ASP), 303
- Nota, A., Livio M., Clampin M., & Schulte-Ladbeck R. 1995, ApJ, 448, 788
- Owocki, S. P., Cranmer S. R., & Gayley K. G. 1996, ApJ, 472, L115
- Paczyński, B., & Ziółkowski, J. 1968, Acta Astron., 18, 255, 735
- Parks, G. K. 1991, in Physics of Space Plasmas: An Introduction (New York: Addison-Wesley)
- Peimbert, M. 1978, in IAU Symp. 76, Planetary Nebulae: Observations and Theory, ed. Y. Terzian (Dordrecht: Reidel), 215
- Różyczka, M., & Franco, J. 1996, ApJ, 469, L127
- Schmidt, G. 1989, in IAU Coll. 114, White Dwarfs, ed. G. Wegner (Dordrecht: Kluwer), 305
- Stone, J. M., & Norman, M. L. 1992, ApJS, 80, 753
- Schwarz, H. E., Aspin, C., Corradi, R. L. M., & Reipurth, B. 1997, A&A, 319, 267
- van Genderen, A. M., & Thé, P. S. 1984, Space Sci. Rev., 39, 317
- Vishniac, E. T. 1983, ApJ, 274, 152
- _____. 1994, ApJ, 428, 186
- Wagenhuber, J., & Weiss A. 1994, A&A 290, 807
- White, S. 1997, in ASP Conf. Ser. 120, Luminous Blue Variables: Massive Stars in Transition, ed. A. Nota & H.J.G.L.M. Lamers, (San Francisco: ASP), 320